Chemical Physics 367 (2010) 83–92

Contents lists available at ScienceDirect

Chemical Physics

journal homepage: www.elsevier.com/locate/chemphys

Fluorescence spectroscopic behaviour of folic acid

A. Tyagi, A. Penzkofer *

Institut II – Experimentelle und Angewandte Physik, Universität Regensburg, Universitätstrasse 31, D-93053 Regensburg, Germany

ARTICLE INFO

Article history:
Received 7 September 2009
In final form 28 October 2009
Available online 1 November 2009

Keywords:
Folic acid
Absorption cross-section spectra
Fluorescence excitation spectra
Fluorescence quantum distributions
Fluorescence lifetimes
Photo-induced proton release
Intra-molecular electron transfer
9,10-Dehydro-folic acid

ABSTRACT

The fluorescence spectroscopic behaviour of folic acid (FA) in 4 M HCl (dominant bi-cationic form), 0.1 M HCl (bi-cationic and cationic form), citric acid–NaOH pH 6 buffer (neutral form), 0.1 M and 4 M KOH (anionic form), and trifluoroacetic acid is studied. The thermal stability is investigated. Absolute absorption cross-section spectra are determined and compared with fluorescence excitation spectra. Intrinsic fluorescence quantum distributions and fluorescence quantum yields are extracted from fluorescence spectra measurements. The temporal fluorescence decay after picosecond pulse excitation is studied. The fluorescence quenching mechanisms for the different ionic forms of FA are discussed: excited-state proton release for bi-cationic FA, photo-physical non-radiative relaxation for cationic FA, and photo-induced intra-molecular electron transfer for neutral and anionic FA. Aerobic FA in 4 M KOH at elevated temperature dehydrated to 9,10-dehydro-folic acid. Its photo-dynamics was governed by twisted intra-molecular charge transfer and photo-isomerisation.

1. Introduction

Folic acid (pteroylglutamic acid, abbreviated as FA) is a widely distributed vitamin (called vitamin B_C, vitamin M, or vitamin B_9). It is involved in single carbon transfer reactions in metabolism, and it is the precursor of the active tetrahydrofolic acid coenzyme [1]. It was first discovered in spinach [2]. Folic acid deficiency causes growth weakness in mammals and different kinds of anaemia; it causes a failure to make the purines and thymine required for DNA synthesis [3]. FA is a potential agent for cancer prevention [4,5] by free radical scavenging and antioxidant activity [6]. FA is made up of the building blocks pterin, p-amino-benzoic acid, and glutamic acid. Folate is the preferred name of folic acid and folic acid derivatives.

The chemistry and biochemistry of folates and pterins is reviewed in [1,7,8]. Depending on the pH of aqueous solutions, folic acid exists in different ionic states. The structural formulae of FA in neutral, anionic, cationic, and bi-cationic form are shown in Fig. 1 [9]. The change from the neutral form to the anionic form occurs with a dissociation constant of $pK_{n,a} = 8.38$ [9], the change from neutral form to cationic form has a dissociation constant of $pK_{n,c} = 2.35$, and the pK value for the transformation from cationic form to bi-cationic form was reported to be $pK_{c,bc} = 0.20$ [9]. The pK values of the α-carboxyl group and of the γ-carboxyl group of the glutamic acid part have not yet been determined [9]. They are expected to be similar to the pK values of free glutamic acid in aqueous solution ($pK_\alpha = 2.1$ and $pK_\gamma = 4.07$ [10]). Absorption spectra of FA in its different ionization states are found in [1,7–9,11,12]. Fluorescence studies on folic acid were carried out in [13–19]. No fluorescence was found in [13,14]. pH dependent fluorescence behaviour was reported in [15] where fluorescence spectra are shown for pH 2, 5, 6, 7, 8, and 9. Fluorescence quantum yields were found to be less than 0.005 in [16,17] for acid and basic forms of FA. Fluorescence quenching processes are discussed in [16,18–20]. The photo-stability of FA was studied in [1,8,16,19,21–26].

In this paper a fluorescence spectroscopic characterization of FA in 4 M aqueous HCl (pH ≈ −0.6, dominant bi-cationic folate), 0.1 M aqueous HCl (pH ≈ 1, mixture of cationic and bi-cationic folate), aqueous citric acid-NaOH pH 6 buffer (neutral folate), 0.1 M aqueous KOH (pH ≈ 13, anionic folate), 4 M KOH (pH ≈ 14.6, anionic folate), and trifluoroacetic acid (TFA, $pK = 0.5$ [27]) is undertaken. The thermal stability of FA in these solvents is studied. Fluorescence emission spectra, fluorescence excitation spectra, and temporal fluorescence decay traces are measured. The fluorescence quantum distributions, $E_F(\lambda)$, and the fluorescence quantum yields, ϕ_F, are calculated by calibration to standard reference dyes. Fluorescence lifetimes are extracted from temporal fluorescence traces obtained by picosecond laser pulse excitation and streak-camera or micro-channel-plate photomultiplier signal detection. Schemes of the photo-dynamics are derived from the experimental results. The fluorescence behaviour of bi-cationic folate is interpreted in terms

* Corresponding author. Tel.: +49 941 943 2107; fax: +49 941 943 2754.
E-mail address: alfons.penzkofer@physik.uni-regensburg.de (A. Penzkofer).

0301-0104/$ - see front matter © 2009 Elsevier B.V. All rights reserved.
doi:10.1016/j.chemphys.2009.10.026

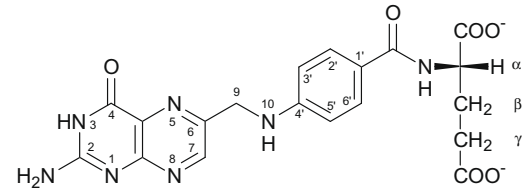

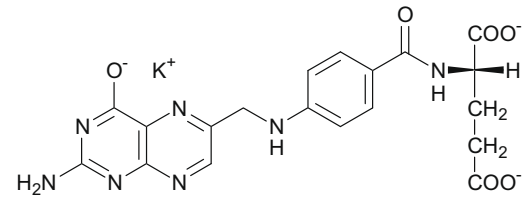

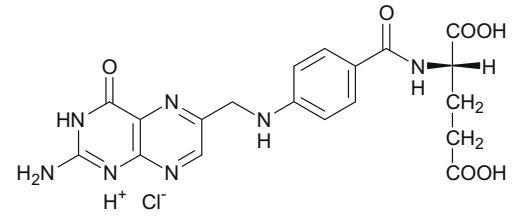

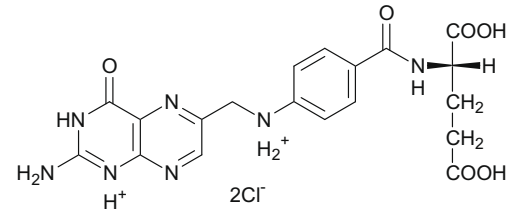

Fig. 1. Structural formulae of folic acid in neutral (sum formula: $C_{19}H_{19}N_7O_6$, molar mass M_m = 441.4 g mol^{-1}), anionic, cationic, and bi-cationic form.

of photo-induced proton release and subsequent thermal activated internal conversion. For cationic folate a temperature independent non-radiative decay is found. For neutral folate and anionic folate the fluorescence is thought to be quenched by intra-molecular electron transfer. Higher excited-state deactivation towards the ground-state via conical intersection are made responsible for excitation wavelength dependent fluorescence quenching (violation of Vavilov's rule of excitation wavelength independent fluorescence quantum yield [28,29] and of Kasha–Vavilov's rule of exclusive fluorescence emission from S_1 state with efficiency independent of the excitation wavelength [30]).

2. Experimental

Folic acid (purity $\geqslant$0.985, water content 7.9%) was purchased from Schircks Laboratories, 8645 Jona, Switzerland. The other chemicals were bought from Sigma–Aldrich, Germany, in highest purity quality. The chemicals were used without further purification.

The samples were studied under aerobic conditions (solvents used as delivered). FA was dissolved in 4 M aqueous HCl, 0.1 M aqueous HCl, aqueous citric acid–NAOH pH 6 buffer (commercial solution from Aldrich), 0.1 M aqueous KOH, 4 M aqueous KOH, and in TFA. Additional measurements were carried with FA in Tris–HCl pH 8 buffer (25 mM Tris + 150 mM NaCl + 5 vol.% glycerol, pH adjusted with HCl, Tris = $(HOCH_2)_3CNH_2$).

Folic acid is poorly soluble in aqueous solution at room temperature, but the solubility rises with temperature [1]. Therefore, we dissolved folic acid in the aqueous solvents of different pH at 70 °C and then let the samples cool down to room temperature. The so prepared samples remained dissolved without agglomerisation for a few days. FA is good soluble in TFA. The temporal stability of the samples at room temperature was tested by measuring the absorption spectra after sample preparation in certain time intervals over a period of a few days. No remarkable absorption changes were observed. The dye aggregation was checked by 90° static light scattering experiments [31] using a HeNe laser (λ_L = 632.8 nm) for excitation and a photomultiplier for detection. Centrifuged samples showed approximately the same light scattering as the corresponding solvents. Heating of FA in 4 M HCl reversibly shifted the bi-cationic – cationic equilibrium to the cationic side (rise of long-wavelength absorption, see below). Prolonged heating of FA in TFA caused absorption spectral changes due to thermal degradation (see below). Prolonged heating of FA in 4 M KOH oxidized FA to 9,10-dehydro-folic acid (DHFA, see below).

Absorption cross-section spectra of the samples were determined with a Cary 50 spectrophotometer (from Varian, Darmstadt, Germany). The absorption in the long-wavelength absorption tails was measured using cells of 10 cm length; otherwise cells of 1 cm length were used.

The fluorescence spectra, $S_F(\lambda)$, of the samples were measured with a Cary Eclipse spectrofluorimeter (from Varian). For absolute intrinsic fluorescence quantum distribution, $E_F(\lambda)$, calibration of the samples, the dyes 2-amino-pyridine in 0.1 normal aqueous H_2SO_4 (absorption below 330 nm, fluorescence quantum yield ϕ_F = 0.60 [32,33]), POPOP (1,4-di-(5-phenyloxazolyl)benzene) in ethanol (absorption below 380 nm, ϕ_F = 0.85 [34]), and coumarin 314T in ethanol (absorption below 460 nm, ϕ_F = 0.87% according to data sheet of Kodak) were used as fluorescence standards. The fluorescence was collected perpendicular to the excitation path. The samples were excited with vertical polarized light, and the fluorescence polarized to the magic angle (54.7° to the vertical) with a polarizer was detected. The fluorescence quantum yield, ϕ_F, is obtained by integration over the fluorescence quantum distribution, i.e. $\phi_F = \int E_F(\lambda)d\lambda$.

Fluorescence excitation spectra, $E_{ex,\lambda_{det}}(\lambda)$, were also determined with our Cary Eclipse spectrofluorimeter by collecting the fluorescence at a fixed emission wavelength of λ_{det} and scanning the excitation wavelength λ through the absorption region [35]. $E_{ex,\lambda_{det}}(\lambda)$ is defined as $E_{ex,\lambda_{det}}(\lambda) = S_{F,m}(\lambda_{det})/P_{in}(\lambda) = \kappa[1 - T(\lambda)]\phi_F(\lambda)$ where $S_{F,m}(\lambda_{det})$ is the magic-angle fluorescence signal at the detection wavelength, $P_{in}(\lambda)$ is the excitation power, $T(\lambda) = \exp[-\alpha(\lambda)\ell]$ is the transmission (α: absorption coefficient, ℓ: sample length), $\phi_F(\lambda)$ is the fluorescence quantum yield belonging to the excitation wavelength, and κ is a proportionality constant. In the case of high transmission ($T > 0.8$) it is $E_{ex,\lambda_{det}}(\lambda) \approx \kappa'\alpha(\lambda)\phi_F(\lambda) = \kappa''\sigma_a(\lambda)\phi_F(\lambda)$. If the fluorescence quantum yield, ϕ_F, is independent of the excitation wavelength, then the shape of the fluorescence excitation spectrum is equal to the shape of the absorption spectrum $A(\lambda) = 1 - T(\lambda)$, and for high transmissions it is approximately equal to the shape of the absorption cross-section spectrum, $\sigma_a(\lambda)$.

Fluorescence decays of the samples were studied by picosecond laser pulse excitation and time-resolved fluorescence detection. Measurements at room temperature and at liquid nitrogen temperature (77.2 K) were carried out with excitation at 351.3 nm. A mode-locked Nd:phosphate glass laser system [36] with second harmonic generation (in a non-critical phase-matched CDA crystal [37]) and third harmonic generation (frequency mixing of fundamental and second harmonic light in an angle phase-matched

BBO crystal [37]) was used for excitation pulse generation (pulse duration $\Delta t_L \approx 6$ ps, wavelength $\lambda_L = 351.3$ nm). The fluorescence signal was detected with an ultrafast streak-camera (type C1587 temporal disperser with M1952 high speed streak unit from Hamamatsu) [38]. The streak-camera has a time resolution of about 3 ps in the fastest streak speed of 300 ps/15 mm (time window 165 ps), and a time resolution of about 100 ps in the slowest streak speed of 10 ns/15 mm (time window 5 ns). For measurements at 77.2 K the sample cells were purged into an optical glass dewar filled with liquid nitrogen.

Further fluorescence lifetime measurements at room temperature were carried out by sample excitation at 400 nm (pulse duration ca. 4.5 ps) using second harmonic pulses of a Ti:sapphire femtosecond laser oscillator-amplifier system (laser system Hurricane from Spectra Physics) and signal detection with a micro-channel-plate photomultiplier (Hamamatsu type R1564-U01) in combination with a fast digital oscilloscope (LeCroy type DSO 9362).

For picosecond fluorescence excitation at 449 nm our Ti:sapphire laser system was operated at 397 nm and the radiation was red-shifted by stimulated Raman scattering in ethanol (Stokes shift 2928 cm^{-1}) [39] using a Raman generator – amplifier system [40] with two 5 cm cells in series (distance between cells ca. 30 cm for divergence reduction).

3. Results

The absorption cross-section spectra of the samples at room temperature are shown by the thick curves in Fig. 2. The dye concentrations were around 4×10^{-5} mol dm^{-3}. In all cases no vibronic structure is seen indicating an inhomogeneous broadening of the transitions. The shapes of the spectra depend on the pH of the aqueous solutions (ionicity of the folates). The main absorption band of FA in 4 M HCl peaks at 320 nm. A weak absorption plateau is present in the 360–430 nm region. FA is dominantly present in bi-cationic form. The long-wavelength absorption plateau is attributed to the presence of some FA in single-cationic form. The absorption spectrum of FA in TFA is similar to the absorption spectrum of FA in 4 M HCl. In 0.1 M HCl, FA is present in single cationic and bi-cationic form (see below). The absorption strength, $\int[\sigma_a(\lambda) \setminus \lambda]d\lambda$, of the first absorption band is moderate. The absorption cross-section spectrum of FA in citric acid–NaOH pH 6 buffer (neutral folate form) has a weak absorption band around 440 nm and a medium absorption band peaking at 345 nm. The long-wavelength absorption band is attributed to charge-transfer state absorption [41,42]. For FA in 0.1 M KOH and 4 M KOH (anionic folate form) the absorption behaviour is similar to the neutral situation. The first absorption band has its maximum at 365 nm. A long-wavelength absorption tail is present.

Heating of FA in 4 M HCl from 22 °C to 85 °C increased the absorption strength of the long-wavelength absorption band ($\lambda > 360$ nm) approximately a factor 1.8. Cooling down the sample brought the absorption back to the original situation. Due to this behaviour we interpret the long-wavelength absorption band of FA in 4 M HCl as originating from cationic FA (heating shifts bi-cationic – cationic equilibrium towards the cationic side, see below).

Heating of FA in TFA irreversibly raised the absorption strength of the long-wavelength absorption band ($\lambda > 360$ nm, no decrease in absorption by cooling down) likely by increasing the fraction of single-cationic FA (FAH^+). The absorption spectrum changes of FA in TFA due to heating up to 65 °C and keeping the sample at this temperature are shown in Fig. 3a. The long-time heating (>8 h) decreased the absorption band centred at 380 nm and decreased more strongly the dominant absorption band centred at 315 nm. The chemical reactions causing thermal degradation are not identified here.

Prolonged heating of FA in 4 M KOH irreversibly converted FA into a new species. The temporal absorption spectrum development at 85 °C is shown in Fig. 3b. The spectra have isobestic points at 381 nm and 298 nm indicating that only one new species was formed. The new species has its absorption maximum at 425 nm and its absorption cross-section there is 5.1×10^{-17} cm^2.

We think that a double bond is formed between C9 and N10 (for numbering see Fig. 1) by the oxidative action of the dissolved

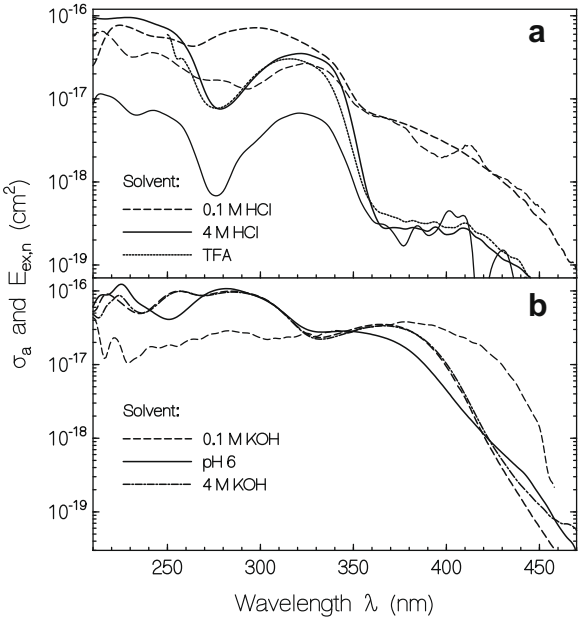

Fig. 2. Absorption cross-section spectra (thick curves) and fluorescence excitation spectra (thin curves, detection wavelength 480 nm, normalized to absorption cross-sections at 370 nm) of folic acid in various solvents. The used solvents are indicated in the figure.

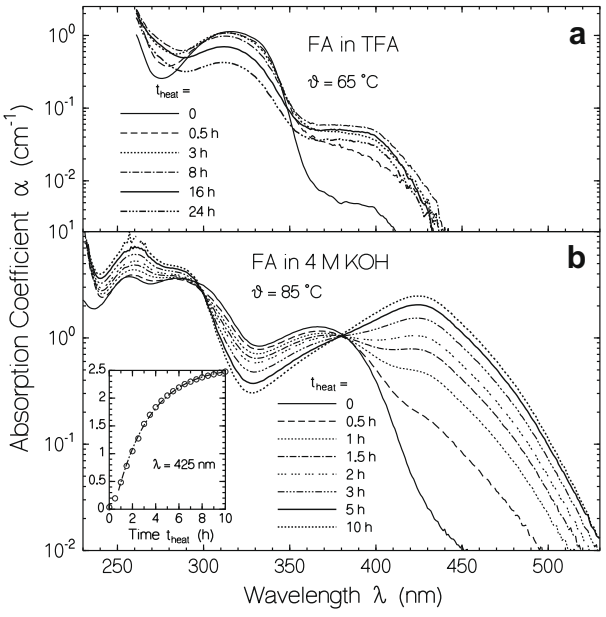

Fig. 3. Development of absorption coefficient spectra due to sample heating. Storage times, t_{heat}, of samples at temperatures ϑ are indicated. (a) FA in TFA at $\vartheta = 65$ °C. (b) FA in 4 M KOH at $\vartheta = 85$ °C. Inset shows absorption coefficient at 425 nm versus heating time.

oxygen under the catalytic action of KOH. The following reaction is thought to take place:

$$FA + O_2 \overset{KOH,85\,^\circ C}{\rightarrow} 9,10\text{-dehydro-FA} + H_2O_2.$$

The inset in Fig. 3b shows the build-up of absorption at 425 nm at 85 °C with time t. The absorption dependence is well fitted by

$$\alpha(t - t_0) = \alpha(t_0)[1 - \exp(-k_1 t)], \quad (1)$$

with a quasi-unimolecular rate constant of $k_1 = 9.4 \times 10^{-5}\ s^{-1}$ (dissolved O_2 concentration is much higher than FA concentration). The consumption of FA is approximately given by

$$\frac{d[FA]}{dt} = -k_2[O_2][FA] = -k_1[FA], \quad (2)$$

with $k_1 = k_2[O_2]$. Heating an anaerobe sample of FA in 4 KOH under the same conditions as the aerobe sample resulted in no absorption spectra changes (no dehydration occurred). In passing, it is noted that a similar dehydration is taking place in the biogenesis of green fluorescent protein [43].

In Fig. 4a–e fluorescence quantum distributions, $E_F(\lambda)$, of FA in the different aqueous solvents and in TFA at room temperature are shown. In each sub-figure $E_F(\lambda)$ curves are shown for several excitation wavelengths. All emission bands are rather broad. They show no vibronic structure. The fluorescence efficiency depends on the excitation wavelength. Vavilov's rule of excitation wavelength independent fluorescence emission efficiency [28,29] is violated for the studied folate samples.

For FA in 4 M HCl and in TFA the main emission band is centred at 485 nm. A short-wavelength emission band centred at 370 nm is additionally resolved in the case of short wavelength excitation. The main emission is attributed to S_1–S_0 emission from single-cationic FA (excited-state proton release, see below), and the short-wavelength emission is attributed to S_1–S_0 emission from bi-cationic FA (see below). For FA in 0.1 M HCl the emission maximum occurs at around 470 nm. No short-wavelength-emission band was resolved. For FA in pH 6 buffer the fluorescence emission peak emission occurs at 445 nm. In the case of long-wavelength-excitation ($\lambda_{exc} \geqslant 400$ nm) the emission maximum shifts to longer wavelength. For FA in 0.1 M KOH the main emission band peaks at 460 nm. Excitation into the long-wavelength absorption tail results in an enhanced red-shifted emission similar to the pH 6 situation. In the case of short wavelength excitation a weak additional emission around 350 nm could be resolved. This weak emission may be due to the presence of some p-amino-benzoic acid fragments [44] and some higher excited state emission.

Fluorescence quantum distributions of FA in TFA which was thermostated at 65 °C for 3 h are displayed in Fig. 5a for different excitation wavelengths. The spectra have their maxima at around 480 nm. The fluorescence quantum yield rises with excitation wavelength.

The fluorescence quantum distributions of FA in 4 M KOH and of 9,10-dehydro-FA (DHFA) in 4 M KOH (aerobe sample kept at 85 °C for 10 h) are displayed in Fig. 5b. The FA spectra have their maxima at around 490 nm, the DHFA spectrum peaks at around 580 nm. The fluorescence quantum yield of FA rises with excitation wavelength ($\phi_F(320\,nm) \approx 0.00036$, $\phi_F(338\,nm) \approx 0.00063$). The fluorescence quantum yield of DHFA is $\phi_F = 0.021 \pm 0.002$.

The excitation wavelength dependence of the fluorescence quantum yield, ϕ_F, of FA in the studied solvents at room temperature is summarized in Fig. 6. The total fluorescence quantum yield, $\phi_{F,tot}$ (thick curves), and the quantum yield of the short wavelength emitted fluorescence, $\phi_{F,short}$ (thin curves), are shown. In all solvents the fluorescence quantum yield varies with excitation wavelength. The highest fluorescence quantum yield in the few percent range was obtained for FA in TFA.

The wavelength dependence of the fluorescence quantum yield is also seen in the fluorescence excitation spectra which are included in Fig. 1 for FA in 4 M HCl, 0.1 M HCl, and 0.1 M KOH (thin curves). For wavelength independent fluorescence quantum yields the presented normalized fluorescence excitation spectra, $E_{ex,n}(\lambda) = E_{ex,480\,nm}(\lambda)\sigma_a(370\,nm)/E_{ex,480\,nm}(370\,nm)$, should coincide with the absorption cross-section spectra, which is not the case. Over the presented wavelength range the sample transmission was kept higher than 70%.

Picosecond-pulse-excited temporal fluorescence traces measured with a streak-camera are shown in Fig. 7 (excitation

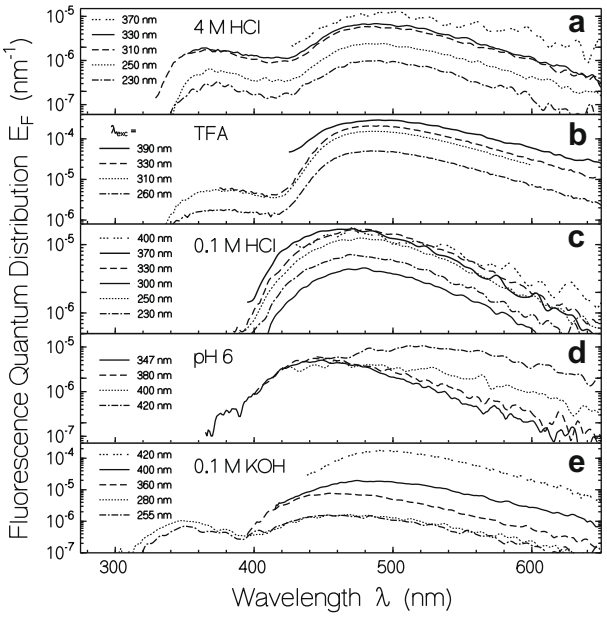

Fig. 4. Fluorescence quantum distributions, $E_F(\lambda)$, of folic acid in studied solvents. Distributions are shown for several excitation wavelengths, λ_{exc}.

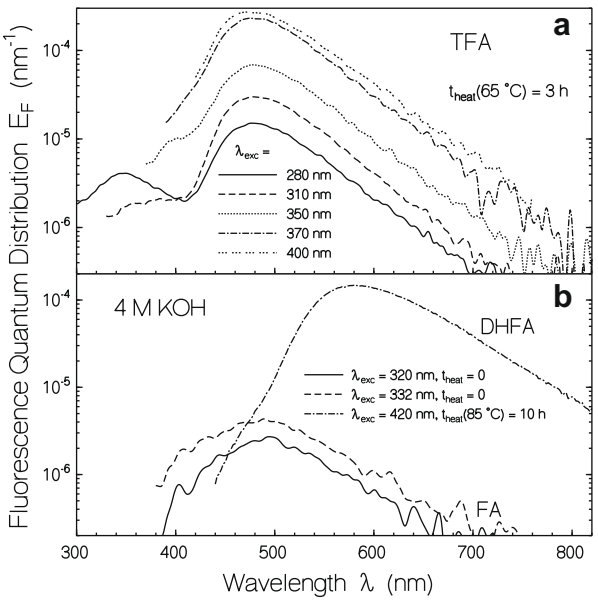

Fig. 5. (a) Fluorescence quantum distributions at room temperature for FA in TFA after 3 h at 65 °C. Curves at different excitation wavelengths are shown. (b) Fluorescence quantum distributions at room temperature for FA in 4 M KOH at fluorescence excitation wavelengths $\lambda_{exc} = 320$ nm and 332 nm, and for 9,10-dehydro-FA (DHFA) at $\lambda_{exc} = 420$ nm (conversion of FA to DHFA by sample storage for 10 h at 85 °C).

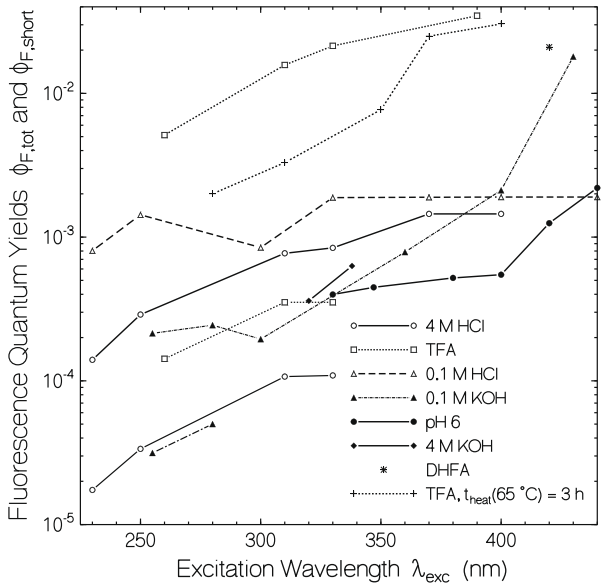

Fig. 6. Fluorescence quantum yields of folic acid in studied solvents versus excitation wavelength. Experimental data points are indicated by symbols. Thick line connected points: total fluorescence quantum yields. Thin line connected points: short-wavelength fluorescence quantum yield contributions.

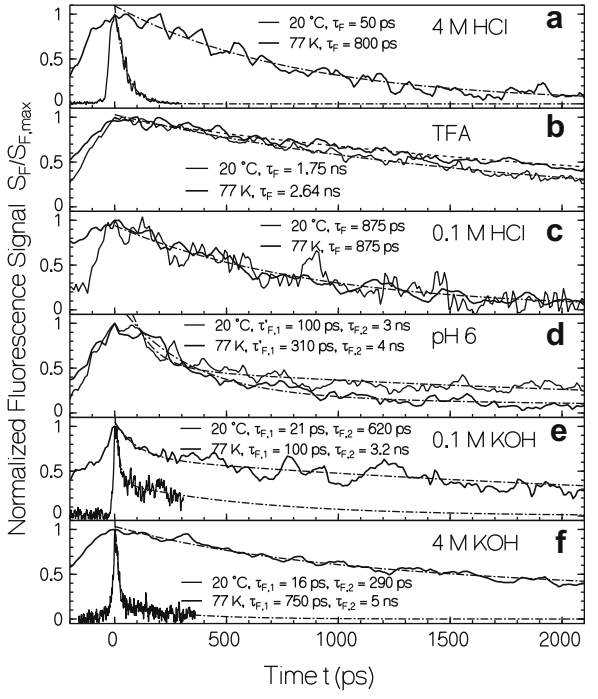

Fig. 7. Temporal fluorescence traces belonging to folic acid in studied solvents. Fluorescence excitation at $\lambda_L = 351.2$ nm with laser pulses of $\Delta t_L \approx 6$ ps duration. Fluorescence light is collected for $\lambda_F \geqslant 435$ nm (Schott filters KV435 in path) in the cases of FA in 4 M HCl, TFA, 0.1 M HCl, 0.1 M KOH, and for $\lambda_F \geqslant 418$ nm (Schott filters KV418 in path) in the case of FA in pH 6 buffer. Thin solid lines belong to measurements at room temperature; thick solid lines belong to measurements at 77.2 K; and dash-dotted curves are exponential regression fit curves. Fitted fluorescence lifetime parameters are listed.

wavelength 351.2 nm, excitation pulse duration ≈ 6 ps). The thin solid curves were measured at room temperature, and the thick solid curves were measured at 77.2 K. The dash-dotted curves are single-exponential or bi-exponential regression fits. The extracted fluorescence decay times are indicated in the part figures. The room temperature results are also listed in Table 1. Fluorescence lifetimes at room temperature were also measured by picosecond pulses excitation at 400 nm and 449 nm where the signal detection occurred with a micro-channel-plate photomultiplier (full half-width of response function ≈ 650 ps). Short fluorescence lifetimes (range of 200 ps to 1 ns) were determined by signal curve de-convolution (the procedure is described in [45]). The results are given in Table 1 using the presentation

$$S_F(t)/S_{F,max} = x_1 \exp(-t/\tau_{F,1}) + x_2 \exp(-t/\tau_{F,2}), \quad (3)$$

where x_1 and x_2 are the fractions of components with fluorescence lifetimes $\tau_{F,1}$ and $\tau_{F,2}$.

The fluorescence of FA in 4 M HCl, in TFA, and in 0.1 M HCl decays single-exponentially. For FA in 4 M HCl (bi-cationic FA) the fluorescence lifetime increased from 50 ps at room temperature to 800 ps at 77.2 K. For FA in TFA the fluorescence lifetime increased from ≈1.75 ns at room temperature to ≈2.6 ns at 77.2 K. For FA in 0.1 M HCl the fluorescence lifetime was found to be $\tau_F \approx 875$ ps independent of the temperature.

For FA in pH 6 buffer (neutral FA) the fluorescence decayed bi-exponentially with a very short component and a slow component in the case of excitation at 351.2 nm. The very short component will be attributed to direct locally-excited-state emission and the slow component will be attributed to delayed locally-excited-state emission and charge-separated-state emission [38]. The time constant of the very short fluorescence component could not be resolved directly from the fluorescence trace in Fig. 7d because of limited time-resolution. Its value will be extracted below by combining the information of fluorescence trace and fluorescence quantum yield measurements. The time constant of the short fluorescence component was longer at 77.2 K than at room temperature indicating a potential energy surface barrier crossing in the excited-state deactivation. In the case of excitation at 400 nm and 449 nm (micro-channel-plate signal detection) the very short

Table 1
Fluorescence lifetimes of folic acid in various solvents at room temperature.

Solvent	λ_{exc} (nm)	x_1	$\tau_{F,1}$ (ns)	x_2	$\tau_{F,2}$ (ns)
4 M HCl					
	351.3	1	0.05		
	400	1	≈0.05		
	449	1	≈0.05		
0.1 M HCl					
	351.3	1	0.88		
	400	1	≈0.9		
	449	1	≈0.9		
pH 6 buffer					
	351.3	≈0.998	0.00023	≈0.002	≈3
	400[a]	≈0.9	1.9	≈0.1	≈7.6
	449[a]	⩽0.06	0.5	⩾0.94	≈2.5
0.1 M KOH					
	351.3	≈0.65	0.021	≈0.35	0.62
	400[a]	1	1.3		
	449[a]	1	1.6		
4 M KOH					
	351.3	1	0.013		
	400[a]	1	0.38		
	449[a]	1	0.43		
	400[b]	1	≈0.6		
TFA					
	351.3	1	1.75		
	400	1	1.8		
	449	1	≈2.6		
	400[c]	0.85	0.4	0.15	4.9

Covered fluorescence spectral region in the case of λ_{exc} = 400 nm and 449 nm was λ_{det} = 501–566 nm (FWHM range).
[a] Shortest time constant could not be resolved (see text).
[b] t_{heat}(85 °C) = 10 h.
[c] t_{heat}(65 °C) = 24 h.

time constant could not be observed because of too low time resolution (its presence is documented by the small fluorescence quantum yield).

The fluorescence decay of FA in 0.1 M KOH and in 4 M KOH (anionic FA) behaved similar as in the case of FA in pH 6 buffer. The short fluorescence component could be time resolved in the streak-camera measurements to be in the 10–25 ps range.

The prolonged heating of FA in 4 M KOH converted it to DHFA. Fluorescence decay traces were measured for excitation at 400 nm. Signal de-convolution allowed the extraction of a fluorescence time constant of $\tau_F \approx 600$ ps. The S_0-S_1 absorption strength (Fig. 3b) gives a radiative lifetime of $\tau_{rad} \approx 24$ ns (lower wavelength limit $\lambda_u = 380$ nm used, see Eq. (8) below) leading to a fluorescence lifetime of $\tau_F \approx 500$ ps ($\phi_F = 0.021$, see Eq. (7) below).

Heating of FA in TFA to 65 °C for 24 h caused bi-exponential fluorescence decay with time constants of ≈400 ps and 4.9 ns (picosecond excitation at 400 nm).

4. Discussion

The spectroscopic behaviour of FA in the different solvents may be put into three groups:

(i) FA in 4 M HCl where FA is dominantly in the bi-cationic form (FAH_2^{2+}); FA in TFA behaves similar to FA in 4 M HCl. The dynamics involves excited-state proton release.
(ii) FA in 0.1 M HCl where FA is partly in the cationic form (FAH^+) and partly in the bi-cationic form. The excited-state deactivation follows photo-physical non-radiative relaxation.
(iii) FA in pH 6 buffer (neutral form) and FA in 0.1 M KOH and 4 M KOH (anionic form, FA^-). The dynamics is dominated by photo-induced intra-molecular electron transfer.

The dehydrated folic acid DHFA in 4 M KOH has a conjugated π electron system extending over the pterin and the imine-benzoic part. The molecules are thought to be present in *trans* and *cis* isomeric form. The photo-excitation dynamics is thought to be determined by *trans* and *cis* state excitation and photo-induced twisted intra-molecular charge transfer.

Quantum chemical semi-empirical PM3 calculation for FA determine permanent dipole moments of $\mu(S_0) = 3.06D$ and $\mu(S_1) = 6.67D$ ($1D = 1$ Debye $= 3.33564 \times 10^{-30}$ C m). These values indicate the polar nature of FA in ground state and the enhanced polar nature in excited state. The calculated dipole moments for DHFA in trans form are of $\mu(S_0) = 6.87D$ and $\mu(S_1) = 9.30D$. The larger dipole moments result from the stretched shape of DHFA in trans form.

The experimental behaviour of FA and DHFA is discussed in the following.

4.1. Folic acid in 4 M HCl and in trifluoroacetic acid

The absorption spectrum of FA in 4 M HCl and in TFA (Fig. 2a) shows a weak absorption pedestal in the 360–430 nm region. The absorption pedestal increases with increasing sample temperature (curves not shown for 4 M HCl, curves for TFA shown in Fig. 3a). The rise of absorption with temperature is reversible for 4 M HCl. It is irreversible for TFA. The fluorescence spectra (Fig. 4a and b) show two emission bands in the case of excitation below 350 nm: a weaker band centred around 370 nm and a stronger band centred around 485 nm. The fluorescence efficiency decreases with decreasing excitation wavelength. The fluorescence signal decay is single exponential ($\lambda_{exc} = 351.3$ nm, 400 nm, 449 nm), and the fluorescence lifetime rises with decreasing temperature.

The absorption and emission behaviour may be understood by (i) bi-cationic FAH_2^{2+} excitation followed by photo-induced proton release [46–48] to cationic FAH^+ and subsequent thermal activated internal conversion from S_1 to S_0 in the case of excitation at wavelength $\lambda_{exc} < 350$ nm, and (ii) by cationic FAH^+ excitation with subsequent thermal activated internal conversion from S_1 to S_0 in the case of excitation at wavelength $\lambda_{exc} > 350$ nm. The photo-dynamics is illustrated by the potential energy scheme presented in Fig. 8a and by the reaction scheme shown in Scheme 1.

In the ground-state there exists a reversible thermal equilibrium between the bi-cationic and the cationic form for FA in 4 M HCl. The fraction of molecules in the cationic form is

$$\rho_{cat} = \exp\left[-\frac{E_g}{k_B\vartheta}\right], \tag{4}$$

where E_g is the energy difference between molecules in the cationic and bi-cationic form, k_B is the Boltzmann constant, and ϑ is the temperature. In the excited state the equilibrium is strongly shifted to the single-cationic form ($pK^*_{c,bc} < pK_{c,bc}$). After photo-excitation of the bi-cationic form (frequency ν_1) there occurs a transfer to the cationic form with a rate of [49,50]

$$k_{PR} = k_0 \exp\left(-\frac{E_{b1}}{k_B\vartheta}\right), \tag{5}$$

where $k_0 \approx k_B\vartheta/h$ is the attempt frequency of barrier crossing [51,52] and E_{b1} is the barrier height in the excited state path from the bi-cationic to the cationic form. h is the Planck constant. Low-frequency excitation (ν_2) directly excites the cationic molecules from their S_0 state to their S_1 state. From there occurs radiative emission (radiative lifetime $\tau_{rad,cat}$), non-radiative intersystem crossing, and dominantly non-radiative internal conversion from the S_1 potential energy surface to the S_0 energy surface via an energy barrier E_{b2}. The rate of thermal activated internal conversion is approximately given by [49,50]

$$k_{IC} = k_0 \exp\left(-\frac{E_{b2}}{k_B\vartheta}\right). \tag{6}$$

From the experimental results some parameters are determined for FA in 4 M HCl (TFA). The fluorescence lifetime of FAH^{+*} was measured to be $\tau_{F,s} \approx 50$ ps (1.75 ns) at room temperature. The fluorescence lifetime is limited by internal conversion. The transfer rate is given by $k_{IC} \approx \tau_{F,s}^{-1}$ leading to $k_{IC} \approx 2 \times 10^{10}\,s^{-1}$ ($5.7 \times 10^8\,s^{-1}$). The barrier height for deactivation is obtained from Eq. (6) to be $E_{b2} = hc_0\tilde{\nu}_{b2} \approx 2.31 \times 10^{-20}$ J or $\tilde{\nu}_{b2} = E_{b2}/hc_0 \approx 1160\,cm^{-1}$ ($1890\,cm^{-1}$).

The radiative lifetime, τ_{rad}, is generally given by

$$\tau_{rad} = \frac{\tau_F}{\phi_F}, \tag{7}$$

where ϕ_F is the fluorescence quantum yield. This relation leads to a radiative lifetime of FAH^{+*} of $\tau_{rad,cat} \approx 36$ ns for FA in 4 M HCl ($\phi_F \approx 0.0014$, $\tau_F \approx 50$ ps) and to $\tau_{rad,cat} \approx 50$ ns for FA in TFA ($\phi_F \approx 0.035$, $\tau_F \approx 1.75$ ns). Knowing the radiative lifetime of the $FAH^{+*} \rightarrow FAH^+$ S_1–S_0 transition, the S_0–S_1 absorption strength, $\bar{\sigma}_a$, of this transition may be determined by application of the Strickler–Berg formula [54–56], which reads in rewritten form:

$$\bar{\sigma}_a = \int_{S_0-S_1} \frac{\sigma_a(\lambda)}{\lambda} d\lambda = \frac{n_A}{8\pi c_0 n_F^3 \tau_{rad}} \frac{\int_{S_1-S_0} E_F(\lambda)\lambda^3 d\lambda}{\int_{S_1-S_0} E_F(\lambda) d\lambda}, \tag{8}$$

where n_A and n_F are the average refractive indices in the S_0–S_1 absorption region and the S_1–S_0 emission region, respectively, and c_0 is the speed of light in vacuum. The obtained results are $\bar{\sigma}_{a,2} \approx 2.83 \times 10^{-18}\,cm^2$ for FA in 4 M HCl ($n_A \approx n_F \approx 1.34$) and $\bar{\sigma}_{a,2} \approx 2.22 \times 10^{-18}\,cm^2$ for FA in TFA ($n_A \approx n_F \approx 1.29$). The experimental absorption strengths, $\bar{\sigma}_{a,2,exp} \approx \int_{S_0-S_1} \frac{\sigma_a(\lambda)d\lambda}{\lambda}$ of the long-wavelength absorption band in Fig 2a are only $\bar{\sigma}_{a,2,exp}$ (4 M

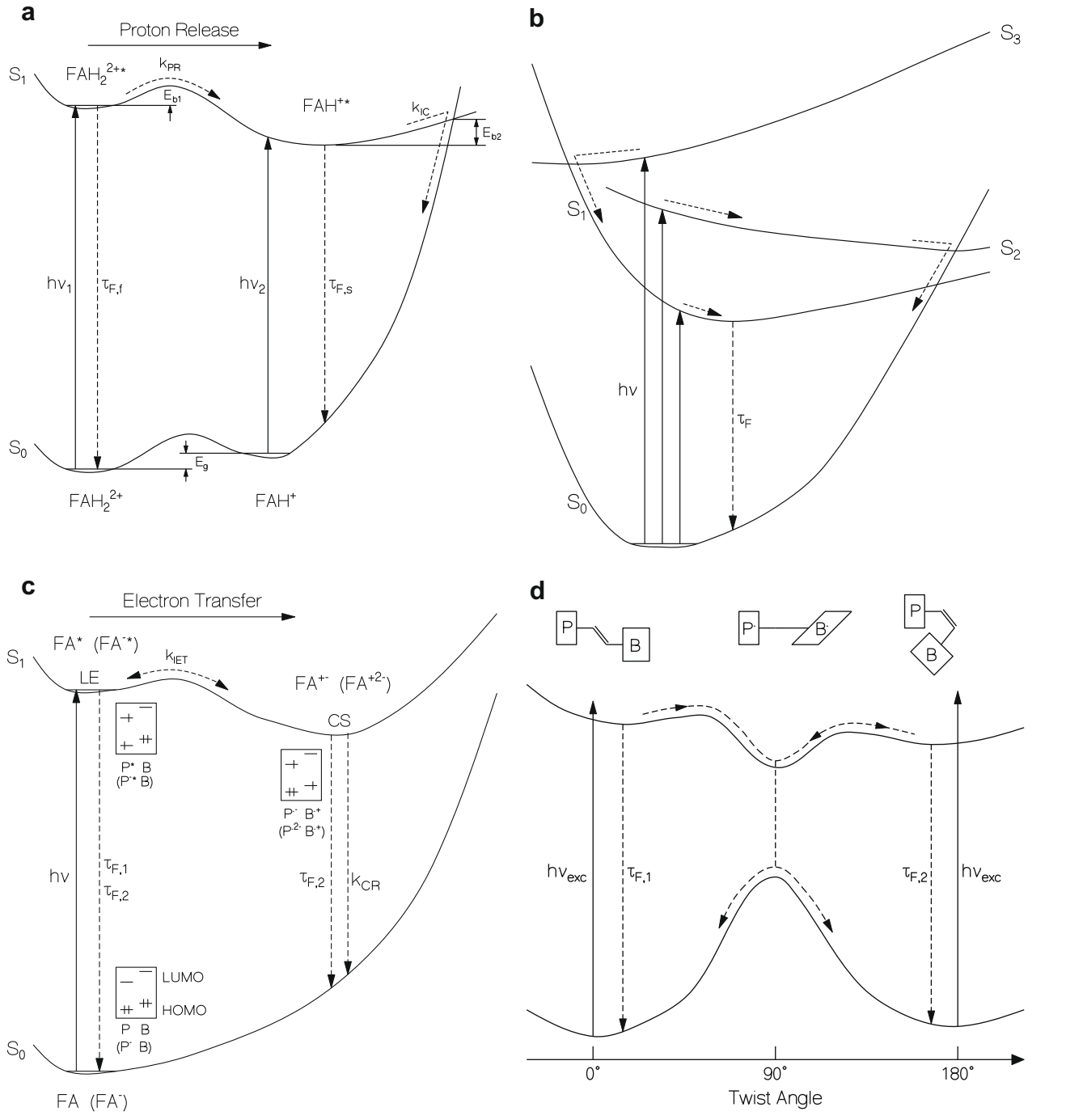

Fig. 8. Potential energy curves and photo-dynamics schemes. (a) Bi-cationic FA relaxation dynamics. (b) Single-cationic FA relaxation dynamics. (c) Neutral and anionic FA relaxation dynamics. (d) Relaxation dynamics of DHFA in 4 M KOH. The scheme is shown for twisted intra-molecular charge transfer and *trans–cis* photo-isomerisation.

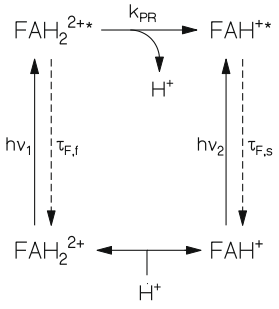

Scheme 1.

HCl) $\approx 4.7 \times 10^{-20}\,\mathrm{cm}^2$ (upper limit of S_0–S_1 absorption set to $\lambda_u = 355$ nm) and $\bar{\sigma}_{a,2,exp}$ (TFA) $\approx 6.5 \times 10^{-20}\,\mathrm{cm}^2$ ($\lambda_u = 355$ nm) because of the limited ground-state population. The fraction of molecules in the cationic state is given by $\rho_{cat} = \bar{\sigma}_{a,2,exp}/\bar{\sigma}_{a,2}$ giving ρ_{cat}(4 M HCl) ≈ 0.023 and ρ_{cat}(TFA) ≈ 0.029. The energy difference between the cationic and bi-cationic form is obtained from Eq. (4) to be $E_g = hc_0\tilde{\nu}_g \approx 1.53 \times 10^{-20}$ J ($\tilde{\nu}_g \approx 770\,\mathrm{cm}^{-1}$) for FA in 4 M HCl and $\tilde{\nu}_g \approx 719\,\mathrm{cm}^{-1}$ for FA in TFA.

The determined fraction, ρ_{cat}, of molecules in the cationic state may be used to estimate the p$K_{c,bc}$ value by application of the Henderson–Hasselblach equation [57] which reads for our situation:

$$\mathrm{pH} = \mathrm{p}K_{\mathrm{c,bc}} + \log\left(\frac{[\mathrm{FAH}^+]}{[\mathrm{FAH}_2^{2+}]}\right). \tag{9a}$$

Rewriting gives

$$\frac{[\mathrm{FAH}^+]}{[\mathrm{FAH}_2^{2+}]} = 10^{(\mathrm{pH}-\mathrm{p}K_{\mathrm{c,bc}})}, \tag{9b}$$

$$\rho_{\mathrm{cat}} = \frac{[\mathrm{FAH}^+]}{[\mathrm{FAH}^+] + [\mathrm{FAH}_2^{2+}]} = \frac{1}{1 + 10^{(\mathrm{p}K_{\mathrm{c,cb}} - \mathrm{pH})}}, \tag{9c}$$

and

$$\mathrm{p}K_{\mathrm{c,bc}} = \mathrm{pH} + \log\left(\frac{1}{\rho_{\mathrm{cat}}} - 1\right). \tag{9d}$$

Insertion of $\rho_{\mathrm{cat}} \approx 0.023$ for FA in 4 M HCl ($\mathrm{pH} \approx -0.6$) gives $\mathrm{p}K_{\mathrm{c,bc}} \approx 1.0$. This value is somewhat larger than the value of 0.2 reported in [9].

The radiative lifetime of FAH_2^{2+*} is obtained from the S_0–S_1 absorption cross-section spectrum of the bi-cationic FA according to the Strickler–Berg relation (Eq. (8)). The result is $\tau_{\mathrm{rad,bicat}}$(4 M HCl) ≈ 12.3 ns (used absorption range from 310 nm to 366 nm) and $\tau_{\mathrm{rad,bicat}}$(TFA) ≈ 15.2 ns (used absorption range from 305 nm to 370 nm). The bi-cationic fluorescence quantum yield is determined from the bi-cationic fluorescence quantum distribution in the short-wavelength range of Fig. 4 (wavelength from 320 nm to 420λ_{exc} = 310 nm) giving $\phi_{\mathrm{F,short}}$(4 M HCl) ≈ 1.1×10^{-4} and $\phi_{\mathrm{F,short}}$(TFA) ≈ 3.5×10^{-4}. The fluorescence lifetimes of the bi-cationic form are obtained by use of Eq. (7) to be $\tau_{\mathrm{F,f}}$(4 M HCl) ≈ 1.35 ps and $\tau_{\mathrm{F,f}}$(TFA) ≈ 5.3 ps. This fluorescence lifetime is determined by the rate of photo-induced proton release which is $k_{\mathrm{PR}} \approx \tau_{\mathrm{F,f}}^{-1}$ giving k_{PR}(4 M HCl) ≈ 7.4×10^{11} s^{-1}, and k_{PR}(TFA) ≈ 1.9×10^{11} s^{-1}. For thermal activated excited-state proton release activation barriers (Eq. (5)) of $\tilde{\nu}_{\mathrm{b1}}$ (4 M HCl) ≈ 520 cm^{-1} and $\tilde{\nu}_{\mathrm{b1}}$ (TFA) ≈ 710 cm^{-1} are estimated.

4.2. Folic acid in 0.1 M HCl

The absorption spectrum (Fig. 2a) shows a moderate absorption band in the 350–450 nm region. The fluorescence spectra show only one emission band. The fluorescence quantum yield for excitation at 370 nm (S_0–S_1 transition) is $\phi_{\mathrm{F}} \approx 0.0019$. The fluorescence efficiency is lower in the case of excitation around 300 nm (S_0–S_2 transition), and it is higher in the case of excitation around 250 nm (S_0–S_3 transition). The fluorescence decay is single exponential, and the fluorescence lifetime is approximately the same at 20 °C and 77.2 K.

The absorption and emission behaviour of the cationic folic acid (FAH^+) in 0.1 M aqueous HCl may be understood by the photodynamics scheme of Fig. 8b. Depending on the excitation wavelength a transition occurs from the S_0 ground-state to a Franck–Condon level in the first (S_1), second (S_2), third (S_3), or higher excited singlet state. S_0–S_1 excitation results in thermally relaxed S_1–S_0 emission with a fluorescence lifetime of $\tau_{\mathrm{F}} \approx 875$ ps. The fluorescence lifetime is thought to be limited by photo-physical non-radiative relaxation by equipotential internal conversion and intersystem crossing [58,59]. No barrier crossing is relevant since the fluorescence lifetimes are the same at room temperature and at 77.2 K (energy barrier for thermal activated internal conversion via S_1–S_0 potential energy surface crossing too high). The rate of non-radiative relaxation is estimated to be $k_{\mathrm{nr}} \approx \tau_{\mathrm{F}}^{-1} \approx 1.1 \times 10^9$ s^{-1}. The S_1–S_0 radiative lifetime is estimated to be (Eq. (7)) $\tau_{\mathrm{rad}} \approx 460$ ns. For excitation into the second excited singlet band (around 300 nm) the fluorescence efficiency is reduced. This behaviour may be understood by partial S_2–S_0 internal conversion via a conical intersection [53,60,61]. Excitation into the next higher singlet band (around 250 nm) results in an increase of the fluorescence efficiency. It is thought that some S_3–S_1 internal conversion via a conical intersection takes place.

In 0.1 M HCl ($\mathrm{pH} \approx 0.1$) FA exists in cationic and bi-cationic form. The S_0–S_1 absorption strength of the cationic form is obtained by application of Eq. (8) to be $\bar{\sigma}_{\mathrm{a,cat}} \approx 1.36 \times 10^{-18}$ cm^2 ($\tau_{\mathrm{rad}} \approx 460$ ns). The experimental S_0–S_1 absorption strength of Fig. 2a (λ_{u} = 355 nm) gives $\bar{\sigma}_{\mathrm{a,cat,exp}} = \int_{S_0-S_1} \frac{\sigma_{\mathrm{a}}(\lambda)d\lambda}{\lambda} \approx 6.9 \times 10^{-19}$ cm^2. The fraction of FA in cationic state is found to be $\rho_{\mathrm{cat}} = \bar{\sigma}_{\mathrm{a,cat,exp}}/\bar{\sigma}_{\mathrm{a,cat}} \approx 0.51$. Insertion of this value into Eq. (9d) gives $\mathrm{p}K_{\mathrm{c,bc}}$ = 0.99 in good agreement with the data analysis for FA in 4 M HCl.

Since for FA in 0.1 M HCl only about 50% of the molecules are present in single-cationic form, the true S_0–S_1 absorption cross-section spectrum of FAH^+ in the wavelength region ⩾360 nm is approximately a factor of two larger than shown in Fig. 2a.

In the case of excitation below 350 nm both cationic and bi-cationic FA are excited. Again photo-induced proton transfer in the excited state is expected to occur as described above for FA in 4 M HCl.

No photo-induced electron transfer is observed for FA in 4 M HCl (cationic pterin and cationic p-amino-benzoic group) and for FA in 0.1 M HCl (cationic pterin group). The positive charged pterin group avoids an electron take-up in the excited state.

4.3. Folic acid in neutral and anionic form

Folic acid in aqueous solution at pH 6 is present in neutral form (FA). Appropriate application of Eq. (9c) gives mole fractions of $\rho_{\mathrm{neutral}} \approx 0.996$ and $\rho_{\mathrm{anionic}} \approx 0.004$ ($\mathrm{p}K_{\mathrm{n,a}}$ = 8.38). For FA in 0.1 KOH ($\mathrm{pH} \approx 13$) and 4 M KOH ($\mathrm{pH} \approx 14.6$) the anionic FA content is ρ_{anionic}(0.1 M KOH) ≈ $1 - 2.4 \times 10^{-5}$ and ρ_{anionic}(4 M KOH) ≈ $1 - 6 \times 10^{-7}$. The absorption spectra (Fig. 2b) reveal weak long-wavelength absorption tails which are thought to be due to charge-transfer state absorption [41,42]. The same overall photodynamics is thought to be going on for FA in neutral and anionic form in the studied solutions.

For FA in pH 6 solution excitation at room temperature at λ_{exc} = 347 nm (S_0–S_1 transition) resulted in a fluorescence spectrum with emission maximum at 445 nm and a fluorescence quantum yield of ≈4.5×10^{-4}. The temporal fluorescence trace (Fig. 7d, λ_{exc} = 351.2 nm) revealed a fast component (lifetime <100 ps) and a slow component (lifetime ≈3 ns). It is assumed that the fast fluorescence component is due to direct locally-excited-state emission and that the slow component is due to delayed locally-excited-state emission and charge-separated-state emission [38].

The radiative lifetime of the S_1–S_0 transition of neutral FA in pH 6 buffer is obtained by application of Eq. (8) (Strickler–Berg formula). The result is $\tau_{\mathrm{rad}} \approx 21$ ns (λ_{u} = 330 nm). A bi-exponential fluorescence trace fit according to $S_{\mathrm{F}}(t)/S_{\mathrm{F,max}} = \kappa_{\mathrm{F,1}} \exp(-t/\tau'_{\mathrm{F,1}}) + \kappa_{\mathrm{F,2}} \exp(-t/\tau_{\mathrm{F,2}})$ (see Eq. (3)) gives $\kappa_{\mathrm{F,1}}$ = 0.482, $\tau'_{\mathrm{F,1}} = 100$ ps, $\kappa_{\mathrm{F,2}}$ = 0.495, $\tau_{\mathrm{F,2}} = 3$ ns. Accordingly the fluorescence quantum yield is composed of two components, i.e. $\phi_{\mathrm{F}} = \phi_{\mathrm{F,1}} + \phi_{\mathrm{F,2}}$. The fast component fluorescence quantum yield, $\phi_{\mathrm{F,1}}$, is obtained from the bi-exponential fluorescence trace in Fig. 7d according to

$$\phi_{\mathrm{F,1}} = \phi_{\mathrm{F}} \frac{S_{\mathrm{F,1}}}{S_{\mathrm{F,tot}}} \approx \phi_{\mathrm{F}} \frac{\kappa_{\mathrm{F,1}} \tau'_{\mathrm{F,1}}}{\kappa_{\mathrm{F,1}} \tau'_{\mathrm{F,1}} + \kappa_{\mathrm{F,2}} \tau_{\mathrm{F,2}}}. \tag{10}$$

Thereby $S_{\mathrm{F,1}}$ is the short component fluorescence signal, and $S_{\mathrm{F,tot}}$ is the total fluorescence signal. The analysis gives $\phi_{\mathrm{F,1}} \approx 1.1 \times 10^{-5}$. The short fluorescence lifetime, $\tau_{\mathrm{F,1}}$, which was experimentally not resolved, may be obtained from the fluorescence quantum yield, $\phi_{\mathrm{F,1}}$ and the radiative lifetime τ_{rad} (Eq. (7)). The calculated value is $\tau_{\mathrm{F,1}} \approx 230$ fs ($x_1 = \kappa_{\mathrm{F,1}} \tau'_{\mathrm{F,1}}/\tau_{\mathrm{F,1}} \approx 0.998$). The slow fluorescence component with $\tau_{\mathrm{F,2}} \approx 3$ ns is present with a fraction of $x_2 \approx 0.002$.

The strong quenching of the fluorescence emission of FA in aqueous pH 6 buffer is thought to be due to reductive intra-molecular electron transfer from the p-amino-benzoic acid part to the photo-excited pterin part of the molecule. The rate of intra-molecular electron transfer is given by $k_{IET} \approx \tau_{F,1}^{-1} \approx 4.3 \times 10^{12}\,s^{-1}$.

In the fluorescence lifetime measurements at 400 nm and 449 nm with the micro-channel-plate photomultiplier (temporal half-width of response function is 650 ps) the ultrafast direct locally-excited-state emission could not be resolved, but its presence is concluded from the small fluorescence quantum yield. The observed rise in quantum yield with increasing excitation wavelength indicates some facilitation of excited-state deactivation with increasing excitation excess energy.

At 77.2 K the fluorescence decay of FA in pH 6 buffer remained bi-exponential with well resolved short fluorescence time constant. The parameters are $\kappa_{F,1} = 0.87 \pm 0.07$, $\tau_{F,1} = 400 \pm 150$ ps, $\kappa_{F,2} = 0.13 \pm 0.07$, and $\tau_{F,2} = 5 \pm 1$ ns. The rate of intra-molecular electron transfer reduced to $k_{IET} \approx 2.5 \times 10^{9}\,s^{-1}$ indicating a thermal activated barrier crossing.

A reaction coordinate scheme for the photo-excitation dynamics of neutral FA is depicted in Fig. 8c. FA is excited to a locally excited state FA* (LE) in the first excited singlet band S_1. There occurs charge separation to an intra-molecular zwitterionic state FA^{+-} (CS). From there occurs (i) some thermally activated CS → LE back transfer causing locally delayed fluorescence (lifetime $\tau_{F,2}$), (ii) some charge-separated-state emission (lifetime $\tau_{F,2}$), and (iii) non-radiative charge recombination (rate constant $k_{CR} \approx \tau_{F,2}^{-1}$). The involved HOMO and LUMO molecular orbitals of the pterin (P) and the p-amino-benzoic acid (B) parts are indicated.

FA was also studied in aqueous solution at pH 8 using Tris–HCl buffer. In this solvent FA is present in neutral and anionic form (pK = 8.38 [9]). The shape of the absorption spectrum was between the shapes of the pH 6 and 0.1 M KOH spectra (curve not shown). The fluorescence spectra followed the spectra of 0.1 M KOH (curves not shown). The fluorescence quantum yield was measured to be $\phi_F\,(360\,nm) \approx 5 \times 10^{-4}$ at room temperature. The fluorescence decay was bi-exponential as in the case of FA in pH 6 and 0.1 M KOH. The fluorescence lifetimes were the same as for 0.1 M KOH within our experimental accuracy.

In 0.1 M KOH (pH ≈ 13) folic acid is present in anionic form (FA^-). The absorption spectrum shows a slowly decaying absorption tail in the long-wavelength range (>410 nm). The tail absorption is attributed to charge-transfer state absorption. The fluorescence spectra show a dominant emission band around 470 nm and a very weak short-wavelength band around 350 nm. This short-wavelength band may be due to some S_2–S_0 emission and some contribution from p-amino-benzoic acid fragment emission of some degraded folic acid molecules. The fluorescence efficiency is excitation wavelength dependent (Figs. 4e and 6 and fluorescence excitation spectrum in Fig. 2b). It is smallest around $\lambda_{exc} = 300$ nm (S_0–S_2 absorption band) probably due to non-radiative S_2–S_0 deactivation via a conical intersection (see situation of Fig. 8b). The larger fluorescence quantum yield in the case of excitation at 280 nm and 255 nm indicates some S_3–S_1 internal conversion via a conical intersection. The temporal fluorescence trace (Fig. 7e, excitation wavelength $\lambda_L = 351.2$ nm) shows a bi-exponential decay behaviour. The parameters at room temperature are $\kappa_{F,1} = 0.65 \pm 0.1$, $\tau_{F,1} = 21 \pm 6$ ps, $\kappa_{F,2} = 0.35 \pm 0.1$, and $\tau_{F,2} = 620 \pm 100$ ps. As in the case of neutral FA the short fluorescence contribution is thought to be due to direct locally-excited-state emission (longer lifetime indicates a slightly higher barrier for excited-state charge separation). The slow component is attributed to delayed locally excited emission and charge-separated-state emission. At 77.2 K the fluorescence decays bi-exponentially with $\kappa_{F,1} = 0.29 \pm 0.06$, $\tau_{F,1} = 600 \pm 200$ ps, $\kappa_{F,2} = 0.71 \pm 0.06$, and $\tau_{F,2} = 5 \pm 2$ ns. The radiative lifetime of the S_1–S_0 transition of FA is obtained by application of Eq. (8) (Strickler–Berg formula, $\lambda_u = 330$ nm). The result is $\tau_{rad} \approx 17.2$ ns.

FA was also studied in 4 M KOH where FA is also present in anionic form. The fluorescence maximum occurred at 475 nm, and the temporal fluorescence trace decayed bi-exponentially with $\kappa_{F,1} = 0.86 \pm 0.06$, $\tau_{F,1} = 16 \pm 4$ ps, $\kappa_{F,2} = 0.14 \pm 0.06$, and $\tau_{F,2} = 290 \pm 50$ ps. At 77.2 K the fluorescence decayed bi-exponentially with $\kappa_{F,1} = 0.5 \pm 0.1$, $\tau_{F,1} = 800 \pm 300$ ps, $\kappa_{F,2} = 0.5 \pm 0.1$, and $\tau_{F,2} = 6 \pm 2$ ns.

The anionic folic acid, FA^-, follows the same photo-induced intra-molecular charge transfer dynamics as neutral folic acid. FA is locally excited to FA^{-*} (LE). From there occurs direct locally-excited-state emission ($\tau_{F,1}$) and charge separation (rate constant $k_{IET} \approx \tau_{F,1}^{-1}$) to FA^{--+} (CS). The CS state evolves by CS → LE back transfer leading to time-delayed locally-excited-state emission ($\tau_{F,2}$), CS state emission ($\tau_{F,2}$), and CS state charge recombination ($k_{CR} \approx \tau_{F,2}^{-1}$) back to FA^-. The FA^- dynamics is indicated in Fig. 8c in parenthesis.

4.4. 9,10-Dehydro-folic acid in 4 M KOH

Keeping of FA in 4 M KOH at 85 °C for a few hours converted the first absorption band peaking at 367 nm completely and irreversibly to a new absorption band peaking at 425 nm and having a shoulder at 480 nm (see Fig. 3b). The fluorescence shifted to the red with an emission maximum at 580 nm and with a weak shoulder around 490 nm (see Fig. 5b). A fluorescence quantum yield of 0.021 was measured. It is thought that FA is thermally dehydrated to 9,10-dehydro folic acid (DHFA) under aerobic conditions. Under anaerobe conditions no dehydration occurred. Trans and cis isomers are thought to be formed by changing from FA^- with flexible 9,10 single-bond to DHFA with stiff 9,10 double-bond. The red-shift of the absorption spectra is caused by the extension of the double bond conjugation. The large absorption–emission Stokes shift, $\delta\tilde{\nu}_{St} = \lambda_{a,max}^{-1} - \lambda_{F,max}^{-1} \approx 6300\,cm^{-1}$ and the still small fluorescence quantum yield of $\phi_F \approx 0.021$ indicate the occurrence of photo-induced twisted intra-molecular charge transfer (TICT state formation) by excited molecular twist between the pterin part and the imine-benzoyl-glutamate part (bi-radical formation and twist around C9,N10 bond) [62]. The large Stokes shift is thought to be due to major conformation (*trans* or *cis*) to minor conformation (*cis* or *trans*) photo-isomerisation.

A dynamics potential energy scheme for DHFA in 4 M KOH is shown in Fig. 8d. Excitation occurs from a planar *trans* or *cis* S_0 ground-state to a *trans* or *cis* excited singlet state. From there occurs locally excited state emission (LE), a molecular twist (TICT state formation) with excited-state deactivation and some *trans*–*cis* or *cis*–*trans* transfer (photo-isomerisation) followed by relaxed excited-state emission.

5. Conclusions

The fluorescence behaviour of folic acid in aqueous solution and in trifluoroacetic acid was studied. The bi-cationic, cationic, neutral, and anionic forms could be investigated by varying the pH of aqueous solutions. FA is only weakly fluorescent in all ionic forms. The excited-state deactivation mechanisms were found to depend on the ionic state of the samples.

In 4 M HCl solution FA is dominantly present in bi-cationic form. Photo-excitation induced a fast excited-state proton release ($FAH_2^{2+*} \rightarrow FAH^{+*} + H^+$) which was followed by a thermal activated FAH^{+*} excited state relaxation.

In 0.1 M HCl solution FA is present in bi-cationic (FAH_2^{2+}) and single-cationic form (FAH^+). The fluorescence lifetime was determined by photo-physical non-radiative decay (internal conversion and intersystem crossing). The weak fluorescence emission

resulted from the weak S_0–S_1 absorption strength (long radiative lifetime and normal rate of non-radiative decay).

In aqueous solution at pH 6 (neutral form of FA) the fluorescence was found to be strongly quenched by photo-induced intra-molecular electron transfer with subsequent non-radiative charge recombination. The fluorescence behaviour was determined by direct locally-excited-state emission, delayed locally-excited-state emission, and charge-separated-state emission.

In aqueous 0.1 M KOH and 4 M KOH solution (anionic form of FA) the fluorescence quenching behaved similar to the neutral FA situation. The dynamics was again determined by photo-induced intra-molecular electron transfer.

The Kasha–Vavilov's rule of excitation wavelength independent constant S_1–S_0 fluorescence emission due to ultrafast higher excited-state to first excited-state internal conversion was not obeyed because other relaxation paths from higher excited potential energy surfaces like conical intersection funnels exist.

FA in 4 M KOH could be dehydrated under aerobe conditions to 9,10-dehydro-FA at elevated temperatures. The photo-dynamics of DHFA turned out to be determined by twisted intra-molecular charge transfer and photo-isomerisation.

The low fluorescence quantum yield of FA may have advantages in its biological vitamin application by avoiding photo-damage due to the short excited state lifetime. In this respect the situation is similar to the DNA bases which have very short excited state lifetimes due to conical intersection decay paths [63–65].

Acknowledgements

The authors thank the Deutsche Forschungsgemeinschaft (DFG) for support to the Research Group FOR 526 "Sensory Blue Light Receptors" and to the Graduate College GK640/3 "Sensory Photoreceptors in Natural and Artificial Systems". A.P. is grateful to Prof. F.J. Gießibl and Prof. J. Repp for their kind hospitality.

References

[1] R.L. Blakley, The Biochemistry of Folic Acid and Related Pteridines, American Elsevier, New York, 1969.
[2] H.K. Mitchell, E.E. Snell, R.J. Williams, J. Am. Chem. Soc. 63 (1941) 2284.
[3] A. White, P. Handler, E.L. Smith, Principles of Biochemistry, fourth ed., McGraw-Hill, New York, 1968 (Chapter 49).
[4] J.B. Mason, L. Levesque, Oncology 10 (1996) 1727.
[5] Y.-I. Kim, J. Nutr. Biochem. 10 (1999) 66.
[6] R. Joshi, S. Adhikari, B.S. Patro, S. Chattopadhyay, T. Mukherjee, Free Rad. Biol. Med. 30 (2001) 1390.
[7] J.C. Rabinowitz, in: P.D. Boyer, H. Lardy, K. Myrbäch (Eds.), The Enzymes, second ed., vol. 2, Academic Press, New York, 1960.
[8] R.L. Blakley, S.J. Benkovic (Eds.), Folates and Pterins, vol. 1. Chemistry and Biochemistry of Folates, John Wiley and Sons, New York, 1984.
[9] M. Poe, J. Biol. Chem. 252 (1977) 3724.
[10] D. Voet, J.G. Voet, Biochemistry, third ed., Wiley, USA, 2004.
[11] B.L. O'Dell, J.M. Vandenbelt, E.S. Bloom, J.J. Pfiffner, J. Am. Chem. Soc. 69 (1947) 250.
[12] A. Pohland, E.A. Flynn, E.H. Jones, W. Shive, J. Am. Chem. Soc. 73 (1951) 3247.
[13] H.M. Rauen, W. Stamm, K.H. Kimbel, Z. Physiol. Chem. 289 (1952) 80.
[14] B.E. Wright, M.L. Anderson, E.C. Herman, J. Biol. Chem. 230 (1958) 271.
[15] K. Uyeda, J.C. Rabinowitz, Anal. Biochem. 6 (1963) 100.
[16] C. Lorente, A.H. Thomas, Acc. Chem. Res. 39 (2006) 395.
[17] A.H. Thomas, C. Lorente, A.L. Capparelli, M.R. Pokhrel, A.M. Braun, E. Oliveros, Photochem. Photobiol. Sci. 1 (2002) 421.
[18] F.M. Cabrerizo, G. Petroselli, C. Lorente, A.L. Capparelli, A.H. Thomas, A.M. Braun, E. Oliveros, Photochem. Photobiol. 81 (2005) 1234.
[19] C. Lorente, A.L. Capparelli, A.H. Thomas, A.M. Braun, E. Oliveros, Photochem. Photobiol. Sci. 3 (2004) 167.
[20] K. Hirakawa, H. Suzuki, S. Oikawa, S. Kawanishi, Arch. Biochem. Biophys. 410 (2003) 261.
[21] A.H. Thomas, G. Suárez, F.M. Cabrerizo, R. Martino, A.I. Capparelli, J. Photochem. Photobiol. A: Chem. 135 (2000) 147.
[22] O.H. Lowry, O.A. Bessey, E.J. Crawford, L. Biol. Chem. 180 (1949) 389.
[23] M.J. Akhtar, M.A. Khan, I. Ahmad, J. Pharm-Biomed. Anal. 25 (1999) 269.
[24] M.J. Akhtar, M.A. Khan, I. Ahmad, J. Pharm-Biomed. Anal. 31 (2003) 579.
[25] M.K. Off, A.E. Steindal, A.C. Porojnicu, A. Juzeniene, A. Vorobey, A. Johnsson, J. Moan, J. Photochem. Photobiol. B: Biol. 80 (2005) 47.
[26] B.S. Patro, S. Adhikari, T. Mukherjee, S. Chattopadhyay, Bioorg. Med. Chem. Lett. 15 (2005) 67.
[27] D.R. Lide (Ed.), CRC Handbook of Chemistry and Physics, 87th ed., Taylor & Francis Group, London, 2006.
[28] S.I. Vavilov, Phil. Mag. 43 (1922) 345.
[29] S.I. Vavilov, Z. Phys. 42 (1927) 311.
[30] G.N. Lewis, M. Kasha, J. Am. Chem. Soc. 66 (1944) 2100.
[31] A. Penzkofer, J. Shirdel, P. Zirak, H. Breitkreuz, E. Wolf, Chem. Phys. 342 (2007) 55.
[32] R. Rusakowicz, A.C. Testa, J. Phys. Chem. 72 (1968) 2680.
[33] D.F. Eaton, EPA Newslett. 28 (1986) 21.
[34] M. Mardelli, J. Olmsted III, J. Photochem. 7 (1977) 277.
[35] C. Birkmann, A. Penzkofer, T. Tsuboi, Appl. Phys. B 77 (2003) 625.
[36] W. Scheidler, A. Penzkofer, Opt. Commun. 80 (1990) 127.
[37] V.G. Dmitriev, G.G. Gurzadyan, D.N. Nikogosyan, Handbook of Nonlinear Optical Crystals, Springer Verlag, Berlin, 1999.
[38] P. Zirak, A. Penzkofer, T. Mathes, P. Hegemann, Chem. Phys. 358 (2009) 111.
[39] A. Penzkofer, A. Laubereau, W. Kaiser, Prog. Quant. Electr. 6 (1979) 55.
[40] B. Meier, A. Penzkofer, Appl. Phys. B 53 (1991) 65.
[41] M. Klessinger, J. Michl, Excited States and Photochemistry of Organic Molecules, VCH Publishers, New York, 1995.
[42] K.-Y. Chen, C.-C. Hsieh, Y.-M. Cheng, C.-H. Lai, P.-T. Chou, T.J. Chow, J. Phys. Chem. A 110 (2006) 12136.
[43] L. Zhang, H.N. Patel, J.W. Lappe, R.M. Wachter, J. Am. Chem. Soc. 128 (2006) 4766.
[44] A.M. Halpern, B.R. Ramachandran, Photochem. Photobiol. 62 (1995) 686.
[45] Sh.D.M. Islam, T. Susdorf, A. Penzkofer, P. Hegemann, Chem. Phys. 295 (2003) 137.
[46] B. Valeur, Molecular Fluorescence. Principles and Applications, Wiley-VCH, Weinheim, 2002.
[47] M. Kasha, in: W.A. Glass, M.N. Varma (Eds.), Physical and Chemical Mechanisms in Molecular Radiation Biology, Plenum Press, New York, p. 231.
[48] A. Müller, H. Ratajczak, W. Junge, E. Diemann (Eds.), Electron and Proton Transfer in Chemistry and Biology, Elsevier, Amsterdam, 1992.
[49] G.R. Fleming, Chemical Applications of Ultrafast Spectroscopy, Oxford University Press, New York, 1986.
[50] J. Schmidt, A. Penzkofer, J. Chem. Phys. 91 (1989) 1403.
[51] M.G. Evans, M. Polanyi, Trans. Faraday Soc. 31 (1935) 875.
[52] H. Eyring, J. Chem. Phys. 3 (1935) 107.
[53] N.J. Turro, V. Ramamurthy, J.C. Scaiano, Principles of Molecular Photochemistry. An Introduction, University Science Books, Sausalito, CA, 2009.
[54] S.J. Strickler, R.A. Berg, J. Chem. Phys. 37 (1962) 814.
[55] J.B. Birks, D.J. Dyson, Proc. R. Soc. Lond. Ser. A 275 (1963) 135.
[56] A.V. Deshpande, A. Beidoun, A. Penzkofer, G. Wagenblast, Chem. Phys. 142 (1990) 123.
[57] R. de Levie, J. Chem. Edu. 80 (2003) 146.
[58] R.M.A. Wandruszka, R.J. Hurtubise, Anal. Chim. Acta 93 (1977) 331.
[59] R.T. Parker, R.S. Freelander, E.M. Schulman, R.B. Dunlap, Anal. Chem. 51 (1979) 1921.
[60] F. Bernardi, M. Olivucci, M.A. Robb, Chem. Soc. Rev. 20 (1996) 321.
[61] D.R. Yarkony, Rev. Mod. Phys. 68 (1996) 985.
[62] Z.R. Grabowski, K. Rotkiewicz, W. Rettig, Chem. Rev. 103 (2003) 3899.
[63] M. Daniels, W. Hauswirth, Science 171 (8) (1971) 675.
[64] W. Domcke, D. Yarkony, H. Köppel (Eds.), Conical intersections: Electronic Structure, Dynamics and Spectroscopy, World Scientific, Singapore, 2004.
[65] C.E. Crespo-Hernández, B. Cohen, P.M. Hare, B. Kohler, Chem. Rev. 104 (2004) 1977.